



# Ferromagnetic cluster spin waves in molecular disks studied by inelastic neutron scattering

J. Nehr Korn,<sup>1</sup> S. Mukherjee,<sup>2</sup> S. Stuibler,<sup>1</sup> H. Mutka,<sup>3</sup> Th. Strässle,<sup>4</sup> G. Christou,<sup>2</sup> and O. Waldmann<sup>1</sup>

<sup>1</sup>Physikalisches Institut, Universität Freiburg, D-79104 Freiburg, Germany

<sup>2</sup>Department of Chemistry, University of Florida, Gainesville, Florida 32611, USA

<sup>3</sup>Institut Laue-Langevin, 6 rue Jules Horowitz, BP 156, F-38042 Grenoble Cedex 9, France

<sup>4</sup>Laboratory for Neutron Scattering, Paul Scherrer Institut, CH-5232 Villigen PSI, Switzerland

(Received 2 August 2012; published 19 October 2012)

Structurally, the two mixed-valence manganese disks Mn<sub>7</sub>-11 and Mn<sub>7</sub>-16 differ only in the peripheral ligand but, as a result of a subtle interplay of intramolecular exchange interactions, differ strongly in their magnetic properties, e.g., Mn<sub>7</sub>-11 possesses a ground-state spin of  $S = 11$  and Mn<sub>7</sub>-16 of  $S = 16$ . The exchange interactions in the disks were studied by inelastic neutron scattering. The analysis of the  $Q$  dependence of the observed magnetic transition intensities reveals that ferromagnetic cluster spin-wave excitations were observed. In this framework, it was possible to successfully model the experimental data and provide a physical understanding of the magnetism in the two disks.

DOI: 10.1103/PhysRevB.86.134417

PACS number(s): 75.50.Xx, 75.45.+j, 75.30.Ds

## I. INTRODUCTION

Molecular nanomagnets (MNM) have attracted the interest of physicists and chemists during the last decades because of their sometimes spectacular magnetic properties. Examples include the slow magnetic relaxation and quantum tunneling of the magnetization exhibited by single-molecule magnets (SMMs), as was first observed in Mn<sub>12</sub>ac,<sup>1,2</sup> quantum phase interference effects,<sup>3</sup> quantum dynamics of the Néel vector,<sup>4-7</sup> and spin frustration effects.<sup>8-11</sup> MNMs contain a few (typically 4 to 20) magnetic metal centers, which are linked together by organic ligands such that each molecule forms a well-defined magnetic nanocluster. Although MNMs incorporate only a relatively small number of interacting spin centers, the lattices are large enough to support complex quantum many-body states.<sup>12</sup> The interpretation of the magnetism can in fact be challenging since MNMs can not be treated as simple paramagnets and not as infinite systems either. In several cases, the adaption of many-body concepts developed for extended systems to these finite (“small”) clusters led to interesting new physics, such as that of quantized spin waves.<sup>13-20</sup> In addition to spin excitations, the ground-state spin  $S$  is also a particularly interesting property of a MNM since it is relevant, e.g., to potential applications.<sup>21</sup> It is a longstanding goal to manipulate this property in a controlled manner,<sup>22-24</sup> and a deeper understanding of the subtle interplay of the magnetic interactions between spin centers and the resulting ground-state spin is desirable.

Disk-shaped magnetic clusters, in which a central magnetic metal ion is encircled by six further ions arranged on the vertices of a hexagon (see Fig. 1), have appeared as common magnetic cores for MNMs. The majority of reported disks are homometallic mixed-valence clusters incorporating metal ions such as Co, Mn, or Fe, but also some monovalent Fe<sup>III</sup> and Co<sup>II</sup> disks have been described (see Refs. 25–27 and references cited therein). In this work, mixed-valence Mn<sub>3</sub><sup>III</sup>Mn<sub>4</sub><sup>II</sup> disks (or Mn<sub>7</sub> disks in short) will be considered, in which a Mn<sup>II</sup> (spin  $S_i = 5/2$ ) ion is sitting at the center, and the remaining three Mn<sup>II</sup> ( $S_i = 5/2$ ) and Mn<sup>III</sup> ( $S_i = 2$ ) ions are positioned alternately on the outer hexagon.<sup>28-32</sup> The large majority of Mn<sub>7</sub> disks possess a ground-state spin of  $S = 11$ , which can

be rationalized as follows: The spins on the six outer ions are aligned parallel to each other but antiparallel to the spin on the central ion, as indicated in Fig. 1(a). This explanation in terms of a classical spin structure is consistent with comprehensive analyses, which include magnetostructural considerations and density functional theory (DFT) calculations.<sup>31-33</sup> It results from dominating ferromagnetic couplings between the spins on the hexagon and weaker couplings to the central spin, which can be ferromagnetic and/or antiferromagnetic, but such that the antiferromagnetic character wins.

Recently, the disk (NH<sub>4</sub>)<sub>3</sub>[Mn<sub>7</sub>(N<sub>3</sub>)<sub>6</sub>(mda)<sub>6</sub>], or Mn<sub>7</sub>-11 in short, which possesses a  $S = 11$  ground-state spin, was synthesized and characterized by magnetization measurements (mda = methyldiethanolamine).<sup>33</sup> Most interestingly, the replacement of the peripheral mda ligands by teaH (teaH = triethanolamine) resulted in the disk (NH<sub>4</sub>)<sub>3</sub>[Mn<sub>7</sub>(N<sub>3</sub>)<sub>6</sub>(teaH)<sub>6</sub>], or Mn<sub>7</sub>-16 in short, which exhibits the maximum possible ground-state spin of  $S = 16$ , as determined from magnetization measurements.<sup>33</sup> In the classical spin structure, all seven spins are thus aligned parallel to each other, as sketched in Fig. 1(b), indicating that the ferromagnetic couplings to the central spin now win. It is unusual that the very small structural changes induced by a ligand exchange in the periphery lead to such significant changes in the magnetic properties. The ground-state spin was found for both molecules to not change under applied pressure, indicating that the effect is rather robust.<sup>34</sup> These findings motivated this work, which reports a study of the low-temperature excitations by means of inelastic neutron scattering (INS) in order to understand the exchange-coupling situation better. INS is renowned as a versatile experimental tool for investigating exchange couplings in MNMs.<sup>12,35,36</sup>

The work was further motivated by the potential to understand the low-temperature physics in Mn<sub>7</sub>-16 in terms of ferromagnetic cluster spin waves. The concept of ferromagnetic spin waves was developed in the early days of quantum mechanics and has since been applied with great success to extended systems,<sup>37-47</sup> but only few examples exist where this concept has been applied to small spin clusters such as MNMs.<sup>13</sup> In contrast to extended systems, however,

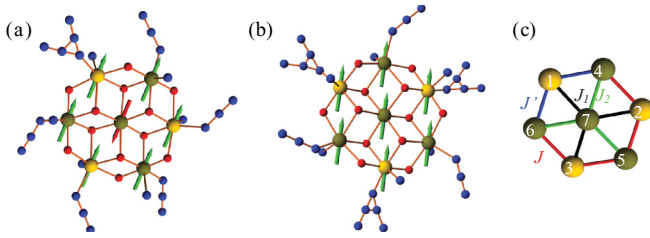


FIG. 1. (Color online) Ball-and-stick representation of the magnetic cores of (a)  $\text{Mn}_7\text{Na-11}$  and (b)  $\text{Mn}_7\text{Na-16}$ , which are analogous to the disks  $\text{Mn}_7\text{-11}$  and  $\text{Mn}_7\text{-16}$ , respectively ( $\text{Mn}^{\text{II}}$ : green,  $\text{Mn}^{\text{III}}$ : yellow, O: red, N: blue; C and H atoms are omitted). Additionally, the classical spin configuration in the respective  $S = 11$  and 16 ground states is depicted by green and red arrows. (c) Exchange-coupling constants used in the magnetic modeling.

characteristic differences appear for small clusters (small as compared to extended systems). First, instead of a treatment in momentum space, the small clusters have in general to be handled in real space since the spin lattice of a small cluster is in general not related to or expandable into an extended lattice (and a Fourier transformation is not obvious).<sup>48</sup> Furthermore, the excitation spectrum consists of relatively few excitations, and spin waves in the sense of dispersive low-energy modes do not exist. In those cases in which the spin lattice is the finite-size version of an extended lattice, the resulting excitations could be described as quantized or discrete spin-wave excitations,<sup>15,16</sup> but such lattices are exceptional and not the rule. Small clusters allow for many spin-lattice topologies, and most of them do not exhibit translation invariance. However, linear ferromagnetic spin-wave theory works for any small ferromagnetic cluster, and in order to distinguish the situation from the extended systems, we prefer to denote the resulting excitations as cluster spin waves (and the real-space theory as ferromagnetic cluster spin-wave theory, FCSWT). An interesting case of a lattice which exists as small and as extended is the ferromagnetic Heisenberg ring (FHR), which expands into the infinite chain. The FHR allows the study of the relation between the momentum-space spin-wave theory and FCSWT. However, experimental studies of the excitations in small FHRs are very scarce; to the best of our knowledge, only the excitations in a  $\text{C}_{10}^{\text{III}}$  wheel have been investigated so far, but not analyzed using FCSWT.<sup>49</sup>

## II. EXPERIMENTS

### A. Molecules

The compounds  $\text{Mn}_7\text{-11}$  and  $\text{Mn}_7\text{-16}$  were synthesized following the procedures described in the literature.<sup>33</sup> Some structural details will be relevant for the magnetic modeling below. The materials were characterized by elemental analysis, IR spectra, and magnetic measurements; x-ray crystallography could not successfully be performed. However, on the basis of these experiments, the magnetic cores in  $\text{Mn}_7\text{-11}$  and  $\text{Mn}_7\text{-16}$  are very similar to those in the analogous compounds  $[\text{Mn}_7(\text{N}_3)_6(\text{mda})_6]\text{Na}(\text{MeOH})_3$  and  $[\text{Mn}_7(\text{N}_3)_6(\text{teaH})_6]\text{Na}(\text{MeOH})_3$ , or  $\text{Mn}_7\text{Na-11}$  and  $\text{Mn}_7\text{Na-16}$  in short. They differ in their chemical compositions from  $\text{Mn}_7\text{-11}$  and  $\text{Mn}_7\text{-16}$  in the counter ion, but also possess  $S = 11$

and 16 ground states, respectively. Their crystal structures were determined by x-ray crystallography,<sup>33</sup> and the molecular structures are presented in Figs. 1(a) and 1(b), respectively. In both compounds, the peripheral azides ( $\text{N}_3$ ) are disordered. In  $\text{Mn}_7\text{Na-11}$ , one of the six azide ligands is disordered among two positions [Fig. 1(a)], which suggest the presence of two slightly different disks in a 1:1 ratio. In  $\text{Mn}_7\text{Na-16}$ , the cluster exhibits a crystallographic  $C_3$  symmetry, and the disorder is such as to be consistent with that [Fig. 1(b)]. The crystal structure could reflect the presence of several slightly different disks with a molecular symmetry lower than  $C_3$ , or the presence of two slightly different disks, which each exhibit a molecular  $C_3$  symmetry, in a 1:1 ratio. The  $\text{Mn}^{\text{III}}$  ions exhibit the usual Jahn-Teller distortion, giving rise to single-ion anisotropy parameters  $D_{\text{Mn}^{\text{III}}} < 0$  along the Jahn-Teller axes, which lie nearly in the plane of the disks (for details, see Ref. 33). Because of the Na counter ion, a polymeric structure is formed in both materials giving rise to significant intermolecular magnetic interactions. This complication is not present in the compounds  $\text{Mn}_7\text{-11}$  and  $\text{Mn}_7\text{-16}$ , which is why we studied these instead of the Na-containing compounds. As mentioned before, their crystallographic structures are not available, but based on the evidence it is reasonable to assume that they are similar to those of  $\text{Mn}_7\text{Na-11}$  and  $\text{Mn}_7\text{Na-16}$ , respectively, and can give useful hints for the magnetic modeling of the latter.

### B. Experimental details

For the INS experiments, nondeuterated polycrystalline samples of  $\text{Mn}_7\text{-11}$  and  $\text{Mn}_7\text{-16}$  were placed in double-walled hollow aluminum cans. The sample masses were 730 and 1360 mg, respectively. INS spectra were recorded at the direct-geometry time-of-flight disk chopper spectrometer IN5 at the Institut Laue-Langevin (Grenoble, France) at various incoming neutron wavelengths; here, data for  $\lambda = 5.0$  and  $6.5 \text{ \AA}$  are shown. The experimental resolutions at the elastic line were 84 and  $41 \mu\text{eV}$ , respectively. The temperature was varied between  $T = 1.5$  and 100 K. The data were corrected for detector efficiency via a vanadium standard. The experiments gave access to the magnetic excitations up to energies of 2 meV. The same samples were also measured at the direct-geometry time-of-flight spectrometer FOCUS at the Paul Scherrer Institut (Villigen, Switzerland) at smaller wavelengths of  $\lambda = 2.26$  and/or  $3.2 \text{ \AA}$  in order to extend the energy range up to above 10 meV. However, identification of further magnetic excitations in these spectra was prevented by a large nonmagnetic scattering contribution, most likely due to the hydrogens in the nondeuterated samples. In the following, the low-energy data recorded at IN5 are presented. Positive energies correspond to the neutron-energy-loss side.

Variable temperature magnetic susceptibility data, which were collected on powder samples of  $\text{Mn}_7\text{-11}$  and  $\text{Mn}_7\text{-16}$  using a Quantum Design MPMS-XL SQUID susceptometer, were reported and discussed previously in Ref. 33. The data will be used in this work for analysis and modeling.

### C. Results

The integrated temperature-dependent INS spectra recorded on  $\text{Mn}_7\text{-11}$  at an incoming neutron wavelength of

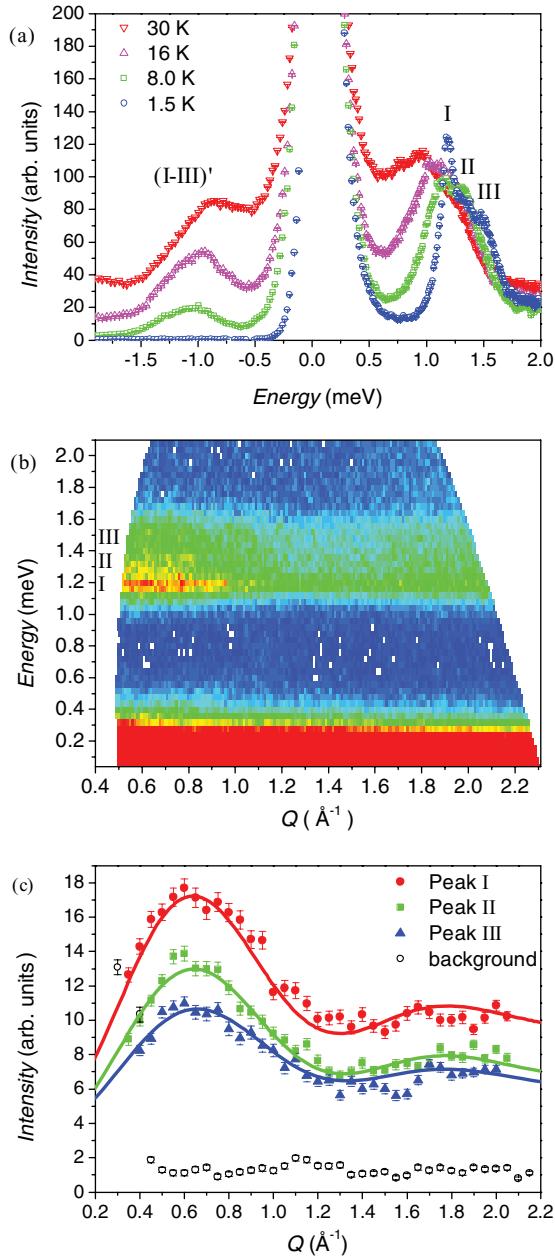


FIG. 2. (Color online) (a) Integrated INS spectra recorded on Mn<sub>7</sub>-11 at an incoming wavelength of  $\lambda = 5.0$   $\text{\AA}$  at the indicated temperatures. (b)  $S(Q, \omega)$  plot of the 1.5-K data. The intensity is color coded from blue (low intensity) to red (high intensity). (c) Experimental  $Q$  dependence of the INS intensity of peaks I, II, and III at  $T = 1.5$  K (solid symbols) and simulated curves (solid lines). In addition, the intensity as function of  $Q$  at an energy of 0.75 meV is shown (open circles), which indicates the nonmagnetic INS contribution. The labels indicate observed peaks.

5.0  $\text{\AA}$  are shown in Fig. 2(a). At a temperature of 1.5 K, three close features are observed on the neutron-energy-loss side: peak I at ca. 1.2 meV, peak II at ca. 1.3 meV, and peak III at ca. 1.45 meV. At higher temperatures, the three features merge into a broad feature with decreased intensity, which is slightly shifted to lower energies. On the neutron-energy-gain side, the expected anti-Stokes peaks are observed as a broad feature at elevated temperatures. The high quality of the data enabled a

detailed study of the momentum transfer ( $Q$ ) dependence of the INS intensity at 1.5 K. The  $S(Q, \omega)$  plot is presented in Fig. 2(b) and the  $Q$  dependencies of the three peaks in Fig. 2(c). For all three peaks, a very similar  $Q$  dependence is observed. At the lowest measured  $Q$  values, the intensity increases with increasing  $Q$ , reaching a maximum at ca. 0.6  $\text{\AA}^{-1}$ . With further increasing  $Q$ , the intensity decreases and stays, within experimental error, almost constant at  $Q$  values higher than ca. 1.2  $\text{\AA}^{-1}$ . On the basis of the temperature and  $Q$  dependence, the three peaks are unambiguously assigned to cold magnetic transitions.

Figures 3(a) and 3(b) show the integrated temperature-dependent INS spectra recorded on Mn<sub>7</sub>-16 at incoming neutron wavelengths of  $\lambda = 6.5$  and 5.0  $\text{\AA}$ . At the lowest measured temperature of 1.5 K, three features are observed on the neutron-energy-loss side at energies of ca. 0.3 (peak I), 1.2 (peak II), and 1.75 meV (peak III). The intensity of peak I decreases strongly with increasing temperature [see Fig. 3(a)], and so do peaks II and III [see Fig. 3(b)]. On the neutron-energy-gain side, the expected anti-Stokes feature related to peak I is observed. The data allowed us to investigate the  $Q$  dependence of the INS intensity at 1.5 K for the three transitions, which are presented in Fig. 3(c). For peak I, the  $Q$  dependence shows a huge intensity at low- $Q$  values, which is due to a known instrumental artifact and shall be ignored. At higher- $Q$  values, a broad and weak maximum at ca. 1.25  $\text{\AA}^{-1}$  is observed. For peaks II and III, the intensity increases at low- $Q$  values, and reaches a maximum at ca. 0.6  $\text{\AA}^{-1}$ . At  $Q$  values larger than ca. 1.3  $\text{\AA}^{-1}$ , the intensity stays constant within experimental errors. On the basis of the temperature and  $Q$  dependence, the three observed peaks are unambiguously assigned to cold magnetic transitions.

To summarize the INS findings, three cold magnetic peaks were observed in both molecules. An analysis using Gaussian fits with appropriate approximations to the nonmagnetic background determined their energy positions to 1.19(1), 1.35(2), and 1.48(2) meV for Mn<sub>7</sub>-11 and 0.30(1), 1.17(2), and 1.72(8) meV for Mn<sub>7</sub>-16.

### III. ANALYSIS

#### A. Spin model and numerical methods

The appropriate spin Hamiltonian for the Mn<sub>7</sub> disks includes a Heisenberg exchange term describing the interactions between the metal ions and an anisotropy term describing the single-ion anisotropy of the Mn<sup>III</sup> ions:

$$\hat{H} = -J \sum_{i=2}^3 \hat{\mathbf{S}}_i \cdot (\hat{\mathbf{S}}_{i+2} + \hat{\mathbf{S}}_{i+3}) - J' \hat{\mathbf{S}}_1 \cdot (\hat{\mathbf{S}}_4 + \hat{\mathbf{S}}_6) - J_1 \sum_{i=1}^3 \hat{\mathbf{S}}_i \cdot \hat{\mathbf{S}}_7 - J_2 \sum_{i=4}^6 \hat{\mathbf{S}}_i \cdot \hat{\mathbf{S}}_7 + D \sum_{i=1}^3 \hat{S}_{i,z}^2. \quad (1)$$

The ions are numbered as shown in Fig. 1(c);  $i = 1, 2, 3$  refer to the Mn<sup>III</sup> centers ( $S_i = 2$ ) and  $i = 4, \dots, 7$  to the Mn<sup>II</sup> ions ( $S_i = 5/2$ ). In a magnetic field, the Zeeman term has to be added (with gyromagnetic factor  $g$ ). The coupling constants  $J$  and  $J'$  describe the exchange interactions between the ions on the outer hexagon, and  $J_1$  and  $J_2$  those involving the central ion [see Fig. 1(c)].  $J, J'$  are ferromagnetic and  $J_1, J_2$  much

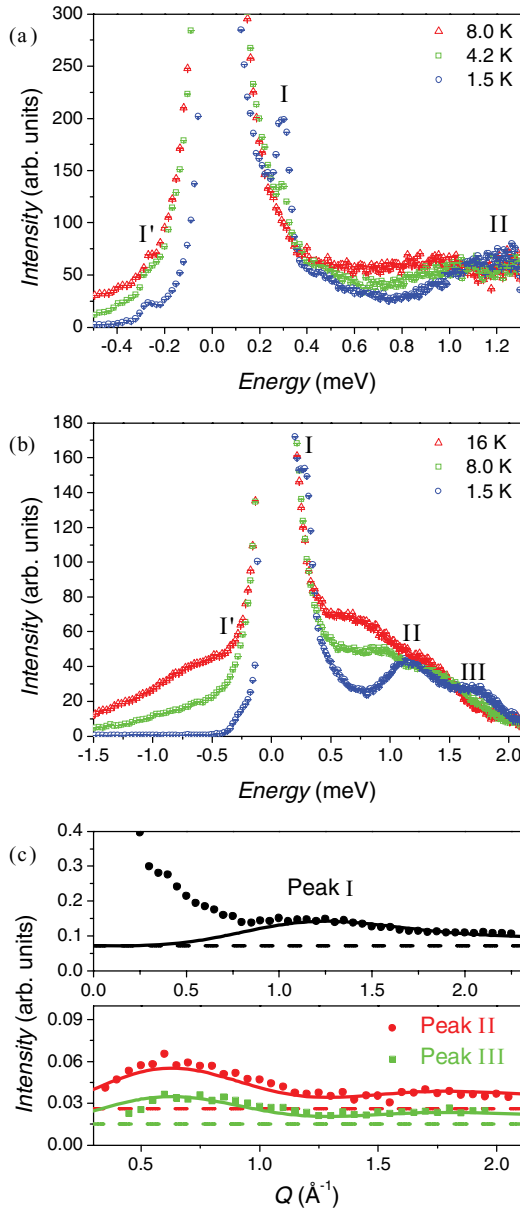


FIG. 3. (Color online) Integrated INS spectra recorded on Mn<sub>7</sub>-16 at an incoming wavelength of (a)  $\lambda = 6.5 \text{ \AA}$  and (b)  $5.0 \text{ \AA}$  at the indicated temperatures. (c) Experimental  $Q$  dependence of the INS intensity of peaks I, II, and III at  $T = 1.5 \text{ K}$  (solid symbols) and simulated curves (solid lines). A constant was added to the simulations (dashed lines) accounting for nonmagnetic scattering contributions. The  $Q$  dependence for peak I was determined from the  $6.5\text{-\AA}$  data, and those of peaks II and III from the  $5.0\text{-\AA}$  data.

weaker, as suggested by previous work.<sup>31–33</sup> In our modeling, the following four exchange models were considered:

(1)  $J$ - $J_1$  model: In this model, two different coupling constants are assumed for describing the interactions along the ring ( $J$ ) and those to the central ion ( $J_1$ ). The magnetic model exhibits  $D_3$  symmetry, and corresponds to  $J' = J$  and  $J_2 = J_1$  in Eq. (1).

(2)  $J$ - $J_1$ - $J_2$  model: In this model, the exchange couplings between the central ion and the Mn<sup>II</sup> ions on the ring ( $J_1$ ) are allowed to be different from those with the Mn<sup>III</sup> ions on

the ring ( $J_2$ ). The magnetic model exhibits  $D_3$  symmetry, and corresponds to  $J' = J$  in Eq. (1).

(3)  $J_a$ - $J_b$ - $J_1$ - $J_2$  model: In this model, additionally a  $J_a$ - $J_b$  modulation of the exchange interactions between the Mn ions on the ring is allowed. The magnetic model exhibits  $D_3$  symmetry, but is not included in Eq. (1) [for the Hamiltonian, see Eq. (A3)]. The parameter space is increased as compared to the  $J$ - $J_1$ - $J_2$  model, but no improvement was found, i.e., a possible  $J_a$ - $J_b$  modulation can not be evidenced with the current experimental data.

(4)  $J$ - $J'$ - $J_1$ - $J_2$  model: In this model, the exchange couplings of one Mn<sup>II</sup> to its neighboring Mn<sup>III</sup> centers ( $J'$ ) is allowed to be different from the other interactions on the ring ( $J$ ) [see Fig. 1(c) and Eq. (1)]. The magnetic model does not exhibit  $D_3$  symmetry. In Mn<sub>7</sub>-11, a  $J$ - $J'$  modulation may be associated to a disordered azide at one of the Mn<sup>II</sup> ions, as suggested by the crystal-structure analysis of the analogous compound Mn<sub>7</sub>Na-11 [see Fig. 1(a)], and DFT calculations of its exchange couplings.<sup>33</sup>

The single-ion anisotropy of the Mn<sup>II</sup> ions was neglected as it is generally much weaker than that of Mn<sup>III</sup>. The anisotropy of the Mn<sup>III</sup> ions was assumed to be equal for the three ions, and to be uniaxial parallel to the disk axis ( $z$  axis) [see Eq. (1)]. The first assumption should be accurate even if the molecule is somewhat distorted and does not exhibit molecular  $C_3$  symmetry. However, the second assumption may not be justified, but had to be introduced to make computations possible within reasonable time; we will address this point carefully in Sec. IV.

The INS intensities were calculated by numerically diagonalizing Eq. (1) to obtain the energies and eigenfunctions and using the formulas given in Refs. 50 and 51. The dimension of the Hilbert space is 162 000. In order to keep the calculations feasible on a personal computer, only the 200 lowest-energy states in each  $M$  subspace were calculated using sparse matrix techniques, where  $M$  denotes the magnetic quantum number associated to the  $z$  component of the total spin. It was carefully checked that the included number of states was sufficient to produce accurate results, even at higher temperatures. By neglecting the anisotropy term, the full energy spectrum of Eq. (1) could be calculated using exact full diagonalization and irreducible tensor operator techniques.<sup>52,53</sup> This facilitated also the simulation of the temperature-dependent magnetic susceptibility. The neglected anisotropy might lead to small deviations at temperatures below a few Kelvins.

### B. Mn<sub>7</sub>-11

The four models presented in the previous section were considered extensively, and the respective parameter spaces were carefully scanned. Only parameter sets consistent with an  $S = 11$  ground state were allowed. However, with the assumption of only one species in the compound, these models did not allow us to reproduce the experimental data. They presented serious discrepancies in that (i) only one or two instead of three INS transitions in the experimental window up to 2 meV were produced, (ii) the  $Q$  dependence of one or more INS peaks did not have a maximum at ca.  $0.6 \text{ \AA}^{-1}$  but rather at  $1 \text{ \AA}^{-1}$  or higher, (iii) the temperature dependence of the INS intensity was wrong, and/or (iv) the magnetic susceptibility was significantly

TABLE I. Magnetic parameters for the two species for both the Mn<sub>7</sub>-11 and Mn<sub>7</sub>-16 disks.

Species	$J/K$	$J'/K$	$J_1/K$	$J_2/K$	$D/K$	$g$
Mn <sub>7</sub> -11						
1	5.2(5)	11.2(5)	2(1)	-2(1)	0.5(2)	1.85(5)
2	5.2(5)	18.0(5)	2(1)	-2(1)	0.5(2)	1.85(5)
Mn <sub>7</sub> -16						
1	5.8(5)	5.8(5)	2.45(100)	-2.00(100)	0.0(3)	2.00(5)
2	8.7(5)	8.7(5)	2.26(100)	-2.00(100)	0.0(3)	2.00(5)

off. The origin of the discrepancies (i) and (ii) is related to the structure of the energy spectrum and nature of the wave functions of Eq. (1) for realistic exchange couplings (exchange on the hexagon much stronger than those to the central ion).

The three models which exhibit at least  $D_3$  symmetry could only produce one INS peak in the energy range of 1.0–1.6 meV since by reasons of symmetry, the two states in this energy range were degenerate. Guided by the crystallographic structure of Mn<sub>7</sub>Na-11, the  $J$ - $J'$ - $J_1$ - $J_2$  model was therefore introduced, which lifts the degeneracy and produces two INS peaks. This model allowed us to reproduce the data in any detail except of the fact that only two of the three INS peaks were accounted for. As the only possible solution to this hurdle we had to assume that the compound contains two, slightly different, species as it is indeed suggested by the structure of the analogous compound Mn<sub>7</sub>Na-11 [Fig. 1(a)]. The determined magnetic parameters are given in Table I. The simulated INS curves are compared to the experimental spectra in Fig. 4(a), and the simulated  $Q$  dependencies are shown in Fig. 2(c). The simulated magnetic susceptibility is presented in Fig. 5. Obviously, the agreement with all data is excellent.

Three points further support this model: First, from the measured INS intensity, the ratio of the two species was estimated to 1:1.4, very close to the expected 1:1 ratio. Second, the simulated intensity of peak I is larger as compared to those of peaks II and III because it is comprised of the contributions of both species, i.e., the energy of the involved transition is nearly identical for both species, while peaks II and III stem from one or the other species [see dashed and dotted lines in Fig. 4(a)]. Simulations showed that the energy of transition I is indeed largely determined by  $J$  and nearly independent of  $J'$ . The larger intensity of peak I is hence perfectly consistent with a two-species model, where the species differ in their  $J'$  exchange bonds because of different azide orientations at one of the Mn<sup>II</sup> ions. And third, the  $Q$  dependence of the INS transition is sensitive to the nature of the wave functions (see Sec. IV). The observation of three (exchange-split) INS peaks with identical  $Q$  dependencies is unusual and their successful modeling is hence strong support for the model.

The energy spectrum produced by the Heisenberg term in Eq. (1) is presented in Fig. 4(b) for the two species as a function of total spin  $S$  ( $D = 0$ ). The anisotropy of the Mn<sup>III</sup> ions produce a zero-field splitting (ZFS) of 4.7 K in the  $S = 11$  ground state, which is comparable to some exchange splittings. However, the energy differences between the  $|M|$  and  $|M + 1|$  subcomponents, which are only probed by INS because of the  $\Delta M = 0, \pm 1$  selection rule, are smaller than 0.8 K and hence

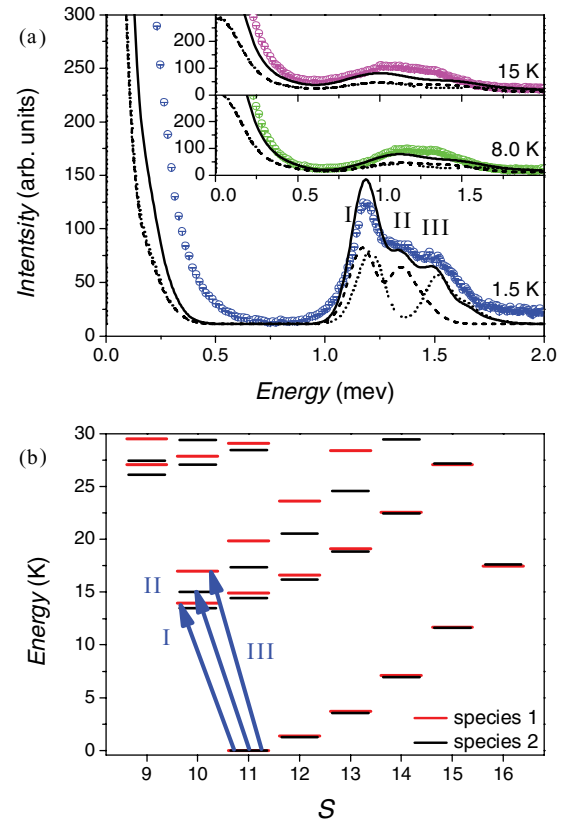


FIG. 4. (Color online) (a) Comparison of simulated and experimental INS spectra on Mn<sub>7</sub>-11 ( $\lambda = 5.0$  Å). The dashed and dotted lines correspond to species 1 and 2, respectively. The solid line corresponds to a mixture of the two species in a ratio of 1:1.4. (b) Energy spectrum (in zero field and with anisotropy neglected) as a function of total spin  $S$  for the two species. Red long bars correspond to species 1 and black short bars to species 2. The three experimental transitions are indicated by the arrows.

not resolved in the INS experiments. The ZFS of the excited states is even smaller than that, which justifies neglecting the anisotropy in a discussion of the energy spectrum.

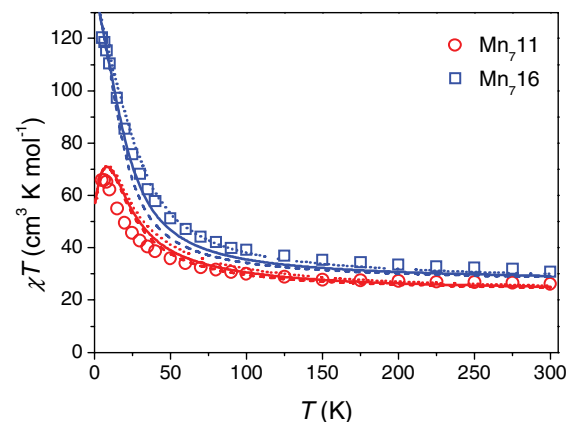


FIG. 5. (Color online) Magnetic susceptibility, plotted as  $\chi T$  vs  $T$ , for Mn<sub>7</sub>-11 (red open circles) and Mn<sub>7</sub>-16 (blue open squares). The solid lines represent the simulated curves; the dotted and dashed lines represent the two species introduced in the modeling for each compound (see text).

The energy spectrum is characterized by several rotational bands [a rotational band is a set of spin multiplets, the energies of which approximately follow the Landé rule  $E(S) \propto S(S+1)$ ].<sup>54–58</sup> The energies in the lowest-lying band were found to be mostly determined by  $J_1$  and  $J_2$ , which is expected from a perturbation theory point of view. This band or a transition from the ground state to the first excited  $S = 12$  multiplet was not observed in our INS experiments, and these transitions must hence be buried in the elastic line and  $J_1$  and  $J_2$  be small in magnitude. It further turned out that  $J_1$  has to be approximately the negative of  $J_2$  as otherwise a peak inconsistent with the INS spectra is obtained. The values of  $J_1$  and  $J_2$  could not be further fixed by the INS data. The magnetic susceptibility, however, was found to be sensitive to them, which allowed their determination, although with significant error bars (see Table I).

At higher energies, two further bands are present in the energy spectrum, which are close to each other. These two bands or the transitions from the  $S = 11$  ground state to the two lowest-lying  $S = 10$  spin multiplets give rise, for each species, to two INS peaks in the energy range of 1–2 meV. For both species together, three peaks are hence observed since the energy of the lowest  $S = 10$  multiplet is similar for both species, as mentioned before. The assignment of the three observed peaks I, II, and III to energy levels is given in Fig. 4(b). The INS spin selection rule  $\Delta S = 0, \pm 1$  allows also transitions from the ground state to the first two excited  $S = 11$  and first two excited  $S = 12$  multiplets, which are at similar energies. However, surprisingly, these are not observed in experiment, and obtained with very weak intensity in the simulated INS spectra. We will come back to this point in Sec. IV B.

### C. Mn<sub>7</sub>-16

Similar to the situation in Mn<sub>7</sub>-11, also for Mn<sub>7</sub>-16 it was found that with assuming one species in the compound, the four models described in Sec. III A did not allow us to reproduce the data by the same reasons of number of INS peaks in the experimental window,  $Q$  and temperature dependence of the INS intensities, and magnetic susceptibility. Hence, guided by the structure of the analogous compound Mn<sub>7</sub>Na-16 [Fig. 1(b)], two species were assumed, where (in contrast to the model for Mn<sub>7</sub>-11) each species was assumed to exhibit molecular  $C_3$  symmetry consistent with the disorder of the azides in Mn<sub>7</sub>Na-16. Each species was modeled by the  $J$ - $J_1$ - $J_2$  model; evidence for a  $J$ - $J'$  modulation as in Mn<sub>7</sub>-11 was not obtained. The magnetic parameters for the two species are given in Table I; a 1:1 ratio was assumed. The simulated INS curves are shown in Fig. 6(a), the simulated  $Q$  dependencies in Fig. 3(c), and the simulated magnetic susceptibility in Fig. 5. Again, the agreement with all data is excellent. For good results, the constants  $J_1$  and  $J_2$  had to be slightly different in magnitude (and opposite in sign), but their absolute values were not precisely fixed by the data, hence the significant error bars in Table I. For Mn<sub>7</sub>-16, the best agreement with data was obtained with negligible single-ion anisotropy  $D = 0.0(3)$  K. However, since transitions related to the anisotropy splitting of spin multiplets were not directly observed, the data are not very sensitive to  $D$  and accordingly the error bar is relatively large.

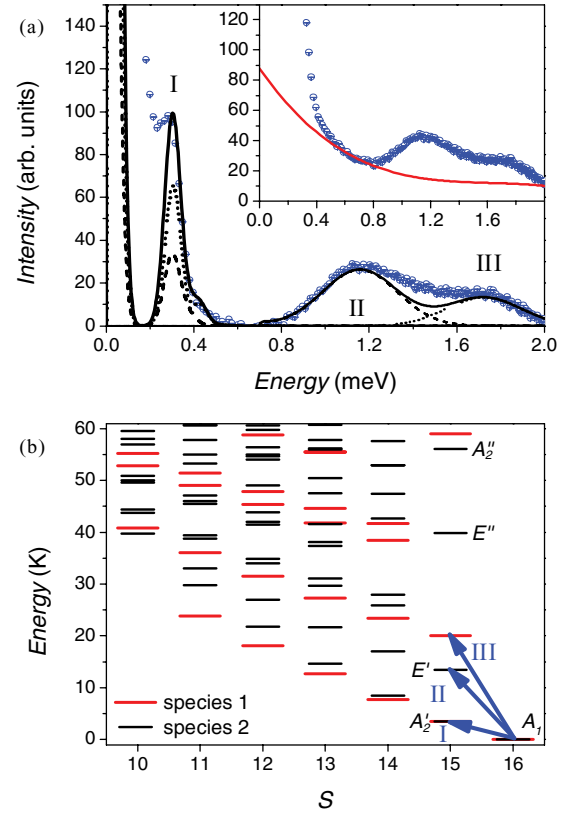


FIG. 6. (Color online) (a) Comparison between simulation and background corrected INS spectrum of Mn<sub>7</sub>-16 ( $\lambda = 5.0$  Å,  $T = 1.5$  K). The dashed and dotted lines correspond to species 1 and 2, respectively. The solid line corresponds to a mixture of the two species in a ratio of 1:1. The inset shows the estimated background. (b) Energy spectrum (in zero field and with anisotropy neglected) as function of total spin  $S$  for the two species. Red long bars correspond to species 1 and black short bars to species 2. The three experimental transitions are indicated by the arrows. The multiplets in the  $S = 15, 16$  sectors are labeled by the irreducible representations of the  $D_3$  symmetry group (for clarity, only the states of one species are labeled).

The linewidth of peak I ( $90 \mu\text{eV}$ ) is slightly larger than the experimental resolution ( $84 \mu\text{eV}$ ), but those of peaks II and III ( $400 \mu\text{eV}$ ) is much larger, probably due to strain effects in  $J$ .

The simulated energy spectrum as a function of  $S$  (for  $D = 0$ ) is displayed in Fig. 4(b) for the two species. The experimentally observed peak I comes from the  $S = 16$  to the lowest  $S = 15$  multiplet transition of both species. Peak II is related to the transition into the first excited  $S = 15$  multiplet of one species and peak III to the same transition of the other species. Since the nature of the wave functions of each of the  $S = 15$  multiplets is different, they give rise to different  $Q$  dependencies (*vide infra*), which is true in particular for the lowest and first excited  $S = 15$  levels. This directly explains why the observed  $Q$  dependence of peak I is different to that of peaks II and III [see Fig. 3(c)], while the similar  $Q$  dependence of peaks II and III strongly supports the two-species model.

As pointed out before in Sec. I, the ground state in Mn<sub>7</sub>-16 assumes the maximal possible spin value of  $S = 16$ , i.e., the ferromagnetic spin multiplet is a ground state. This allows the application of FCSWT, which in linear order yields the energies of the spin excitation in the one-magnon sector or,

in the case of Mn<sub>7</sub>-16, the energies of the multiplets in the  $S = 15$  spin sector. The details of the method when applied to MNMs are described in Ref. 13; its application to Mn<sub>7</sub> disks is given in the Appendix. The FCSWT provided significant guidance in finding the appropriate model parameters in the above analysis. It also provides a detailed understanding of the low-temperature INS excitations (*vide infra*).

## IV. DISCUSSION

### A. Magnetic characterization

From fits to the low- $T$  magnetization curves, the parameters  $D_S = -0.22$  K and  $D_S = -0.03$  K were found in Ref. 33 to describe the  $S = 11$  and 16 ground states in Mn<sub>7</sub>Na-11 and Mn<sub>7</sub>Na-16, respectively. They are negative as expected for Mn<sup>III</sup> ions. Our finding of  $D = 0.5$  K and  $D \approx 0$  for Mn<sub>7</sub>-11 and Mn<sub>7</sub>-16 is consistent insofar as the anisotropy in Mn<sub>7</sub>-11 is much larger than in Mn<sub>7</sub>-16, and very small in the latter. However, the sign appears to be incorrect. This is resolved by noting that the Jahn-Teller axes in these Mn<sub>7</sub> disks, which determine the orientations of the local anisotropy tensors  $\mathbf{D}_i$  of the Mn<sup>III</sup> ions, are almost perpendicular to the disk  $z$  axis (see also Ref. 33). If one assumes that the local anisotropy is uniaxial with a local  $z'$  axis perpendicular to the disk  $z$  axis and has strength  $D_{\text{Mn}^{\text{III}}}$ , and further assumes molecular  $C_3$  symmetry and the strong-exchange limit, then the projection of the local anisotropy tensors on the disk  $z$  axis yields  $D = -\frac{1}{2}D_{\text{Mn}^{\text{III}}}$ . That is, Eq. (1) with the anisotropy term  $\sum_{i=1,2,3} \hat{\mathbf{S}}_i \cdot \mathbf{D}_i \cdot \hat{\mathbf{S}}_i$  instead of  $D \sum_{i=1,2,3} \hat{S}_{i,z}^2$  then produces identical observables. Our results suggest thus  $D_{\text{Mn}^{\text{III}}} \approx -1.0$  K in Mn<sub>7</sub>-11, which is realistic for Mn<sup>III</sup> ions. The ZFS in the  $S = 11$  ground state is calculated to 4.7 K, which relates to  $D_S = +0.04$  K, about five times smaller than the above estimate for Mn<sub>7</sub>Na-11 obtained from the low- $T$  magnetization curves. This discrepancy could reflect the influence of the intermolecular interactions present in Mn<sub>7</sub>Na-11.

Using DFT calculations, the exchange constants in Mn<sub>7</sub>Na-11 and Mn<sub>7</sub>Na-16 were calculated previously.<sup>33</sup> For Mn<sub>7</sub>Na-11, the exchanges on the hexagon were found to be in the range of  $J, J' = 15$ –20 K and those to the central ion to fall into the ranges  $J_2 \approx -2.4$  K and  $J_1 = 1.4$ –2.6 K. For Mn<sub>7</sub>Na-16, the  $J_a$ - $J_b$ - $J_1$ - $J_2$  model was inferred with  $J_a = 14.5$  K,  $J_b = 22$  K,  $J_1 = 2.9$  K,  $J_2 = -1.7$  K. In our experiments on Mn<sub>7</sub>-11 and Mn<sub>7</sub>-16, significantly smaller values for the exchange couplings on the hexagon are obtained, but overall the accuracy of the DFT results is impressive. In particular, the  $J_1$  and  $J_2$  couplings agree well, and therefore our experiments confirm the explanation of the different ground-state spins in terms of a subtle interplay of the  $J_1$  and  $J_2$  exchanges proposed in Ref. 33.

### B. Two-spin model of the excitations

The much stronger exchange interactions between the spins on the hexagon ( $J, J'$ ) as compared to those involving the central spin ( $J_1, J_2$ ) suggests a simplified picture, where the six spins on the hexagon are coupled to one larger spin  $\hat{\mathbf{S}}_R = \sum_{i=1\dots 6} \hat{\mathbf{S}}_i$ , which is then coupled to the central spin  $\hat{\mathbf{S}}_7$ . The hexagon spin  $\hat{\mathbf{S}}_R$  can assume the values  $S_R = 1/2, \dots, 27/2$ , and owing to the ferromagnetic interactions on

the hexagon the ground state belongs to  $S_R = 27/2$ . Excited states are produced by the weaker exchange interactions to the central ion, which in first-order perturbation theory are given by the effective Hamiltonian  $\hat{H}_{27/2} = -J_{27/2} \hat{\mathbf{S}}_R \cdot \hat{\mathbf{S}}_7$  (with  $S_R = 27/2$  and  $J_{27/2} = aJ_1 + bJ_2$ , where  $a, b$  are positive constants and depend on  $J, J'$ ). These excitations could be characterized as “flips” of the central spin, and their energies are mainly governed by  $J_1, J_2$ . Further excited states are obtained by creating flips of the hexagon spin, the lowest of which corresponds to  $S_R = 25/2$  at an excited energy characterized by  $J, J'$  (there are indeed two levels with  $S_R = 25/2$ , in accordance with the standard spin-coupling rules). The weaker exchange interactions to the central ion again produce flip-of-the-central-spin excitations on top of the flip of the hexagon spin.

Within this picture, the structure of the energy spectrum of Mn<sub>7</sub>-11 and its features, Fig. 4(b), are immediately explained, considering that the coupling between the hexagon and the central ion is effectively antiferromagnetic ( $J_{27/2} < 0$ ). In the ground state,  $S_R$  is maximal and the hexagon spin is aligned antiparallel to the central spin. The lowest band of states starting out from the  $S = 11$  ground multiplet, and which go up to the  $S = 16$  multiplet, corresponds to flips of the central spin as described by  $\hat{H}_{27/2}$ . The next higher-lying states, which are the two lowest  $S = 10$  multiplets, correspond to the first flips of the hexagon spin ( $2 \times S_R = 25/2$ ). The branch of states, which starts out from these two multiplets and which extends up to  $S = 15$ , are produced by the flips of the central spin simultaneously with a hexagon spin flip. The scheme can be extended to explain the energies of the further higher-lying multiplets.

This picture of the excitations provides further insight. In Sec. III B, it was noted that the transitions from the  $S = 11$  ground multiplet into the two lowest  $S = 10$  multiplets were observed in the INS experiments, but that the transitions from the ground state into the two excited  $S = 11$  and 12 multiplets in this band of states were not observed and exhibit almost vanishing INS intensity in simulations, although they satisfy the INS selection rules. This is now naturally explained by the fact that the two lowest  $S = 10$  multiplets correspond to only a flip of the hexagon spin, while the other multiplets in this band involve both a flip of the hexagon spin and flip of the central spin. As regards INS intensity, the latter hence correspond to second-order processes with negligible intensity. The validity of this model was checked by inspection of the wave functions. For the discussed multiplets, the wave functions are described to more than 90% by eigenstates of  $\hat{\mathbf{S}}_R$  and  $\hat{\mathbf{S}}_7$  with the respective values for  $S_R$  and  $S_7$ .

It was further noted in Sec. III B that the lowest band of states was not observed in the INS experiments due to its small excitation energies. That is, the observed peaks I, II, and III correspond to flip-of-the-hexagon-spin excitations; flip-of-the-central-spin excitations were not observed. In other words, the INS spectrum is characterized by the excitations on the hexagon, or the excitations of a FHR indeed. As regards our INS experiments, Mn<sub>7</sub>-11 corresponds hence to a FHR (because of the very weak antiferromagnetic interactions between the hexagon and the central spin).

Along these lines, the energy spectrum of Mn<sub>7</sub>-16 can also be rationalized [Fig. 6(b)], with the difference that

the coupling between the hexagon spin and the central ion is effectively ferromagnetic ( $J_{27/2} > 0$ ), yielding an  $S = 16$  ground state. The flips of the central spin give rise to the lowest spin multiplets in the spin sectors  $S = 11, \dots, 15$ . The first flips of the hexagon spin ( $S_R = 25/2$ ) give rise to the second and third excited multiplets in the  $S = 15$  sector, but are in fact degenerate by symmetry. Hence, the observed peak I corresponds to a flip of the central spin, while the observed peaks II and III correspond to flip-of-the-hexagon-spin excitations (for species 1 and 2, respectively). This picture corroborates our previous statement on the different nature of the states involved in peaks I and II, III as reflected by the different INS  $Q$  dependencies in Fig. 3(c).

According to the two-spin model, peaks I, II, III in Mn<sub>7</sub>-11 and peaks II, III in Mn<sub>7</sub>-16 are all excitations on the hexagon or in fact the lowest excitation of the FHR. They are thus of similar physical nature, as is indeed confirmed by their  $Q$  dependencies, which are essentially identical for these five peaks (e.g., they exhibit a maximum at about  $0.6 \text{ \AA}^{-1}$  and a second maximum at ca.  $1.8 \text{ \AA}^{-1}$ ).

### C. Ferromagnetic cluster spin waves

The general method of (linear) FCSWT has been given, e.g., in Ref. 13. For Mn<sub>7</sub>-16, it is worked out in the Appendix. It yields the energies of the states in the  $S = 15$  spin sector, and therefore the low- $T$  excitations, as they were partially also observed in the INS experiment (see Fig. 6). Since Mn<sub>7</sub>-16 consists of seven spin centers, six  $S = 15$  spin multiplets exist.<sup>13</sup> However, because of the  $D_3$  symmetry of the magnetic model, some of them are degenerate. According to group theory, the spectrum consists of two  $A_2$  and two  $E$  irreducible representations, and the levels will be denoted as  $A_2', A_2'', E',$  and  $E''$ ; see also Fig. 6(b). The ferromagnetic ground state belongs to the irreducible representation  $A_1$ .

The physical nature of these states, or ferromagnetic cluster spin waves, can be probed via the  $Q$  dependence of the INS transitions from the ground state into these multiplets. The calculated  $Q$  dependencies, normalized to the maximal scattering intensity, are shown in Fig. 7(a). For comparison, also the  $Q$  dependence of a transition within the  $S = 16$  ground-state multiplet is plotted. The different levels indeed evidence themselves via different  $Q$  dependencies, with, e.g., different positions of the maxima. In particular, the  $E'$  transition is well distinguished. Comparison of the curves in Fig. 7(a) with the experimental  $Q$  dependencies shown in Fig. 3(c) unambiguously identifies peak I as an  $A_2$  cluster spin wave, and peaks II and III as  $E'$  cluster spin waves.

In Sec. IV B, it was found that the observed INS peaks in Mn<sub>7</sub>-11 arise from excitations on the ferromagnetic hexagon of spins, and insofar Mn<sub>7</sub>-11 reduces to a FHR. The (homogeneous) infinite ferromagnetic chain is a textbook example of a system with ferromagnetic spin waves.<sup>59</sup> The dispersion relation is  $\epsilon(k) = 2Js(1 - \cos ka)$ , where  $k$  is the wave vector,  $a$  the lattice constant,  $s$  the length of the spins, and  $J$  the strength of the ferromagnetic Heisenberg interactions. This dispersion law has been confirmed by neutron scattering experiments.<sup>37,38</sup> The excitation spectrum of a homogeneous finite ring (with  $C_N$  symmetry, where  $N$  is the number of spin sites) results from restricting the wave vectors to the allowed values  $Q_q = \pm q \frac{2\pi}{Na}$ ,

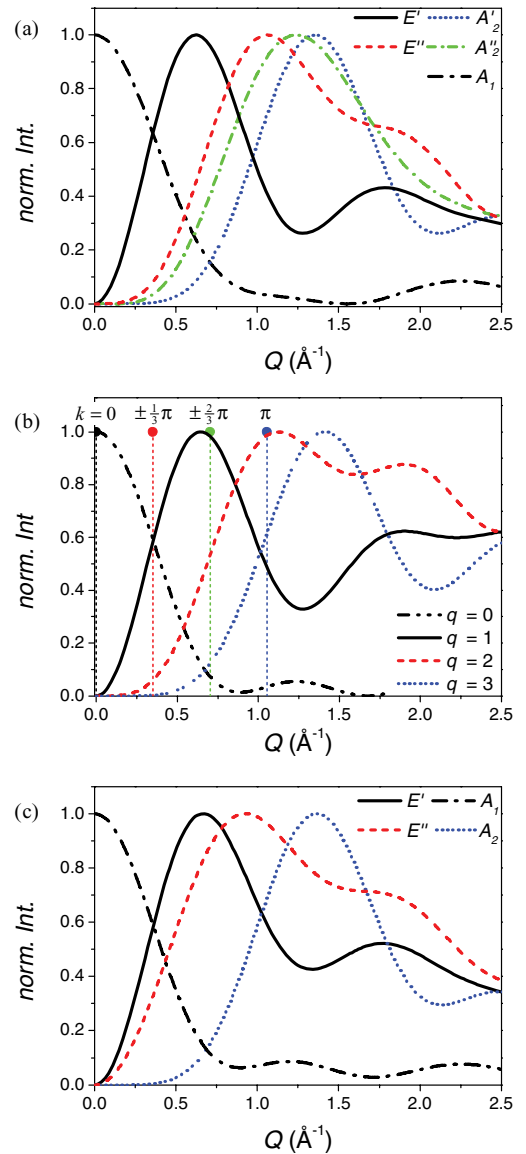


FIG. 7. (Color online)  $Q$  dependence of low-temperature INS transitions, normalized to the maximum for each transition. (a) Mn<sub>7</sub>-16. Transitions are labeled by the irreducible representation ( $D_3$  symmetry group) of the involved excited state. (b) Homogeneous six-membered ferromagnetic Heisenberg ring with  $a = 3.31 \text{ \AA}$ , the average Mn-Mn distance in the considered Mn<sub>7</sub> disks. The magnetic form factor of the ions was set to  $F(Q) = 1$ . Transitions are labeled by  $q$ . The delta-function-like peaks represent the INS intensities for the infinite chain at the excitation energies corresponding to  $k = \pm q\pi/3$ . (c) Six-membered ferromagnetic Heisenberg ring with alternating spins as in Mn<sub>7</sub>-11, but uniform exchange coupling. The ion positions of Mn<sub>7</sub>Na-11 were used in the simulation. Transitions are labeled by the irreducible representation ( $D_3$  symmetry group) of the involved excited state. In all panels, the  $Q$  dependence of a transition within the ground-state multiplet is also shown for comparison, which belongs to  $A_1$  in panels (a) and (c) and  $q = 0$  in panel (b).

where  $q$  is an integer ranging from  $1, \dots, N/2$ . The spectrum hence consists of “quantized” or “discrete” excitations, at exactly the energies given by  $\epsilon(Q_q)$ .<sup>15,16</sup> However, although the energies of the excitations coincide with those of the infinite chain, the INS  $Q$  dependencies are strongly different.

In the infinite chain, the INS intensity peaks at the momentum transfer at which the neutron energy loss equals the dispersion relation (in practice, the delta function is broadened because of lifetime effects). In a small ring, in contrast, the oscillatory  $Q$  dependence typical of small clusters is observed, as shown for a homogeneous six-membered ring in Fig. 7(b). For this case, the  $Q$  dependencies can be calculated analytically, yielding  $I_q(Q) \propto 1 + \frac{1}{6Qa} [12 \cos(\frac{\pi}{3}q) \sin(Qa) + 4\sqrt{3} \cos(\frac{2\pi}{3}q) \sin(\sqrt{3}Qa) + (-1)^q 3 \sin(2Qa)]$ .<sup>51</sup> Moreover, the maxima in the curves do not coincide with the peak positions in the infinite chain but are shifted to larger momentum transfer. With increasing ring size  $N$ , the curves converge to those of the infinite chain, but slowly, i.e., the differences persist for rings of substantial size.

Mn<sub>7</sub>-11 is not a homogeneous ferromagnetic ring because of the  $J$ - $J'$  modulation and the central spin, which complicate matters. It is interesting though to investigate the case of a FHR of alternating Mn<sup>III</sup> and Mn<sup>II</sup> ions with uniform exchange. It can be treated by introducing a larger repeating unit (unit cell) in the calculations. The energies then become  $\epsilon(Q_q) = 2J\bar{s}[1 - \cos(Q_q a)]$ , with the mean spin length  $\bar{s} = 9/4$  per unit cell. The spectrum consists of five cluster spin waves, or three energy levels with degeneracies taken into account. In  $D_3$ , one level belongs to the irreducible representation  $A_2$  and two belong to  $E$ . The  $Q$  dependencies are shown in Fig. 7(c). The  $Q$  dependence of the lowest excitation ( $E'$ ) agrees almost perfectly with the experimental  $Q$  dependencies in Mn<sub>7</sub>-11 [Fig. 2(c)], and furthermore the curves are reminiscent to those for the homogeneous six-membered ring [Fig. 7(b)]. This furthers the notion that the observed excitations in Mn<sub>7</sub>-11 are ferromagnetic cluster spin-wave excitations on the hexagon in nature.

## V. CONCLUSIONS

The low-temperature excitations in the two related Mn<sub>7</sub> disks Mn<sub>7</sub>-11 and Mn<sub>7</sub>-16 were studied by INS experiments. Evidence for the presence of two slightly different species in each compound was found, and magnetic models were established which are in accord with the presumed azide disorder seen in related compounds. The magnetic exchange parameters were deduced, and indications of the single-ion anisotropy of the Mn<sup>III</sup> ions were found. The INS excitations observed in Mn<sub>7</sub>-11 were identified as ferromagnetic cluster spin-wave excitations on the hexagon of the outer Mn<sup>III</sup> and Mn<sup>II</sup> spin centers. The low-temperature excitations in Mn<sub>7</sub>-16 can exactly be calculated using linear ferromagnetic cluster spin-wave theory, and the observed INS transitions interpreted as cluster spin waves. It was demonstrated that the lowest observed INS transition is characterized as a flip of the central spin, while the higher-lying INS transitions correspond to a flip of the total spin on the outer hexagon.

## ACKNOWLEDGMENTS

The authors thankfully acknowledge funding by the Deutsche Forschungsgemeinschaft and USA National Science Foundation. This work is partially based on experiments performed at the Swiss spallation neutron source SINQ, Paul Scherrer Institute, Villigen, Switzerland.

## APPENDIX: FERROMAGNETIC CLUSTER SPIN-WAVE THEORY FOR Mn<sub>7</sub>-16

General equations and results of linear FCSWT are found in Ref. 13. For any small spin cluster, in which Heisenberg interactions stabilize the spin multiplet with maximal total spin  $S_F = \sum_i S_i$  (ferromagnetic ground state), FCSWT enables the exact calculation of the energies and wave functions of the ground state and the excitations in the spin sector  $S = S_F - 1$ . The calculation in fact proceeds in the subspace of the  $M = S_F - 1$  multiplet components, which is of dimension  $N$ . One eigenstate in this subspace belongs to the ferromagnetic ground-state multiplet ( $S = S_F$ ), and hence transforms necessarily as an  $A_1$  irreducible representation. The remaining  $N - 1$  eigenstates belong to the spin sector  $S = S_F - 1$ , which are the cluster spin waves. For Mn<sub>7</sub>-16,

$$|FM\rangle = |M_1 = M_2 = M_3 = 2, M_4 = M_5 = M_6 = M_7 = 5/2\rangle \quad (\text{A1})$$

in an obvious notation.  $M_i$  denotes the eigenvalue of  $\hat{S}_{i,z}$  and the numbering of spin centers follows the scheme in Fig. 1(c). The  $M = S_F - 1$  sector consists of seven states, and a basis is generated by applying the single-ion lowering operators to  $|FM\rangle$ :

$$|i\rangle = \frac{1}{\sqrt{2S_i}} \hat{S}_i^- |FM\rangle. \quad (\text{A2})$$

In the following, the  $J_a$ - $J_b$ - $J_1$ - $J_2$  model will be assumed, which exhibits  $D_3$  symmetry. The Hamiltonian reads as

$$\hat{H} = -J_a \sum_{i=1}^3 \hat{S}_i \cdot \hat{S}_{i+3} - J_b \left( \sum_{i=4}^5 \hat{S}_i \cdot \hat{S}_{i-2} + \hat{S}_6 \cdot \hat{S}_1 \right) - J_1 \sum_{i=1}^3 \hat{S}_i \cdot \hat{S}_7 - J_2 \sum_{i=4}^6 \hat{S}_i \cdot \hat{S}_7 + D \sum_{i=1}^3 \hat{S}_{i,z}^2. \quad (\text{A3})$$

For generality, also a single-ion anisotropy term was included, but  $D \leq 0$  is required for the FCSWT (in Mn<sub>7</sub>-16 we found  $D = 0$ ).

Instead of the  $D_3$  symmetry of the model, it is easier to exploit the  $C_3$  symmetry group (similar to the descent-in-symmetry technique in ligand-field theory).<sup>60</sup> The  $M = S_F - 1$  subspace decomposes into the irreducible representations  $3 \times A + 2 \times E$  in  $C_3$  (and  $1 \times A_1 + 2 \times A_2 + 2 \times E$  in  $D_3$ ). Using standard group-theory procedures,<sup>61</sup> the symmetry-adapted linear combinations (SALCs) are constructed:

$$\begin{aligned} |\alpha_1\rangle &= (|1\rangle + |2\rangle + |3\rangle)/\sqrt{3}, \\ |\alpha_2\rangle &= (|4\rangle + |5\rangle + |6\rangle)/\sqrt{3}, \\ |\alpha_3\rangle &= |7\rangle, \\ |\epsilon_1^\pm\rangle &= (|1\rangle + e^{\pm\varphi i} |2\rangle + e^{\mp\varphi i} |3\rangle)/\sqrt{3}, \\ |\epsilon_2^\pm\rangle &= (|4\rangle + e^{\pm\varphi i} |5\rangle + e^{\mp\varphi i} |6\rangle)/\sqrt{3} \end{aligned} \quad (\text{A4})$$

with  $\varphi = \frac{2}{3}\pi$ . The SALCs corresponding to irreducible representation  $A$  are labeled as  $\alpha$  and those belonging to  $E$

as  $\epsilon$ . The Hamiltonian matrices in the  $A$  and  $E$  subspaces become

$$\begin{pmatrix} 2\kappa + \frac{5}{2}J_2 & -\sqrt{5}\kappa & -\frac{5}{2}\sqrt{3}J_2 \\ -\sqrt{5}\kappa & \frac{5}{2}\kappa + \frac{5}{2}J_1 - 3D & -\sqrt{15}J_1 \\ -\frac{5}{2}\sqrt{3}J_2 & -\sqrt{15}J_1 & 6J_1 + \frac{15}{2}J_2 \end{pmatrix} + E_0 \quad (\text{A5})$$

and

$$\begin{pmatrix} 2\kappa + \frac{5}{2}J_2 & -\sqrt{5}(J_b + e^{-\varphi i} J_a) \\ -\sqrt{5}(J_b + e^{+\varphi i} J_a) & \frac{5}{2}(\kappa + J_1) - 3D \end{pmatrix} + E_0, \quad (\text{A6})$$

where  $\kappa = J_a + J_b$  and  $E_0$  is defined such that the ground-state energy is zero (the matrices for the two components of the irreducible representation  $E$  are identical). The  $E$  matrix is trivially solved. The  $3 \times 3$  Hamiltonian matrix for irreducible representation  $A$  can further be reduced by exploiting  $D_3$  symmetry ( $A \rightarrow 1 \times A_1 + 2 \times A_2$ ). The calculation is straightforward but the results are lengthy and hence not reproduced here. For  $D = 0$ , one can also take advantage of the known (unnormalized) eigenstate  $\sum_i \sqrt{2S_i} |i\rangle$ , which is the  $M = S_F - 1$  component of the  $S = S_F$  ground-state

multiplet:

$$|\alpha'_1\rangle = \frac{1}{4\sqrt{2}}(\sqrt{15}|\alpha_1\rangle + 2\sqrt{3}|\alpha_2\rangle + \sqrt{5}|\alpha_3\rangle). \quad (\text{A7})$$

It is the  $A_1$  eigenstate of the  $3 \times 3$  matrix and has energy  $E = 0$  according to the choice of  $E_0$ . The two remaining basis functions for irreducible representation  $A_2$  are then straightforwardly constructed,

$$\begin{aligned} |\alpha'_2\rangle &= \frac{1}{2}(-|\alpha_1\rangle + \sqrt{3}|\alpha_3\rangle), \\ |\alpha'_3\rangle &= \frac{1}{4\sqrt{2}}(3|\alpha_1\rangle - 2\sqrt{5}|\alpha_2\rangle + \sqrt{3}|\alpha_3\rangle), \end{aligned} \quad (\text{A8})$$

and the corresponding  $2 \times 2$  matrix is obtained:

$$\begin{pmatrix} \frac{1}{2}(\kappa + 9J_1 + 20J_2) & \sqrt{2}(\kappa - 3J_1) \\ \sqrt{2}(\kappa - 3J_1) & 4(\kappa + J_1) \end{pmatrix} + E_0. \quad (\text{A9})$$

Finally, the FCSWT calculation for a six-membered ferromagnetic ring with  $D_3$  symmetry is briefly discussed. The  $M = S_F - 1$  sector consists of six states, which decompose in  $1 \times A_1 + 1 \times A_2 + 2 \times E$  in  $D_3$  or  $2 \times A + 2 \times E$  in  $C_3$ . The  $C_3$  SALCs read as in Eq. (A4) (except of  $|\alpha_3\rangle$  of course). The problem reduces hence to two  $2 \times 2$  matrices for the  $A$  and  $E$  subspaces, respectively, which are trivially solved.

<sup>1</sup>G. Christou, D. Gatteschi, D. N. Hendrickson, and R. Sessoli, *MRS Bull.* **25**, 66 (2000).

<sup>2</sup>D. Gatteschi, R. Sessoli, and J. Villain, *Molecular Nanomagnets* (Oxford University Press, Oxford, UK, 2006).

<sup>3</sup>W. Wernsdorfer and R. Sessoli, *Science* **284**, 133 (1999).

<sup>4</sup>B. Barbara and E. M. Chudnovsky, *Phys. Lett. A* **145**, 205 (1990).

<sup>5</sup>A. Chiolero and D. Loss, *Phys. Rev. Lett.* **80**, 169 (1998).

<sup>6</sup>P. Santini, S. Carretta, G. Amoretti, T. Guidi, R. Caciuffo, A. Caneschi, D. Rovai, Y. Qiu, and J. R. D. Copley, *Phys. Rev. B* **71**, 184405 (2005).

<sup>7</sup>O. Waldmann, T. C. Stamatatos, G. Christou, H. U. Güdel, I. Sheikin, and H. Mutka, *Phys. Rev. Lett.* **102**, 157202 (2009).

<sup>8</sup>U. Kortz, A. Müller, J. van Slageren, J. Schnack, N. S. Dalal, and M. Dressel, *Coord. Chem. Rev.* **253**, 2315 (2009).

<sup>9</sup>C. Schröder, H. Nojiri, J. Schnack, P. Hage, M. Luban, and P. Kögerler, *Phys. Rev. Lett.* **94**, 017205 (2005).

<sup>10</sup>I. Rousochatzakis, A. M. Läuchli, and F. Mila, *Phys. Rev. B* **77**, 094420 (2008).

<sup>11</sup>R. Schmidt, J. Richter, and J. Schnack, *J. Magn. Magn. Mater.* **295**, 164 (2005).

<sup>12</sup>A. Furrer and O. Waldmann [Rev. Mod. Phys. (to be published)].

<sup>13</sup>S. Stuijber, G. Wu, J. Nehrkorn, J. Dreiser, Y. Lan, G. Novitchi, C. E. Anson, T. Unruh, A. K. Powell, and O. Waldmann, *Chem. Eur. J.* **17**, 9094 (2011).

<sup>14</sup>J. Dreiser, O. Waldmann, C. Dobe, G. Carver, S. T. Ochsenein, A. Sieber, H. U. Güdel, J. van Duijn, J. Taylor, and A. Podlesnyak, *Phys. Rev. B* **81**, 024408 (2010).

<sup>15</sup>P. V. Hendriksen, S. Linderth, and P.-A. Lindgård, *Phys. Rev. B* **48**, 7259 (1993).

<sup>16</sup>R. Wieser, E. Y. Vedmedenko, and R. Wiesendanger, *Phys. Rev. Lett.* **101**, 177202 (2008).

<sup>17</sup>S. T. Ochsenein, F. Tuna, M. Rancan, R. S. G. Davies, C. A. Muryn, O. Waldmann, R. Bircher, A. Sieber, G. Carver, H. Mutka *et al.*, *Chem. Eur. J.* **14**, 5144 (2008).

<sup>18</sup>S. Yamamoto and T. Nakanishi, *Phys. Rev. Lett.* **89**, 157603 (2002).

<sup>19</sup>G. Chaboussant, A. Sieber, S. Ochsenein, H.-U. Güdel, M. Murrie, A. Honecker, N. Fukushima, and B. Normand, *Phys. Rev. B* **70**, 104422 (2004).

<sup>20</sup>H. Hori and S. Yamamoto, *Phys. Rev. B* **68**, 054409 (2003).

<sup>21</sup>M. Evangelisti and E. K. Brechin, *Dalton Trans.* **39**, 4672 (2010).

<sup>22</sup>C. J. Milios, S. Piligkos, and E. K. Brechin, *Dalton Trans.* 1809 (2008).

<sup>23</sup>C. J. Milios, R. Inglis, A. Vinslava, R. Bagai, W. Wernsdorfer, S. Parsons, S. P. Perlepes, G. Christou, and E. K. Brechin, *J. Am. Chem. Soc.* **129**, 12505 (2007).

<sup>24</sup>T. C. Stamatatos, K. A. Abboud, W. Wernsdorfer, and G. Christou, *Angew. Chem. Int. Ed.* **46**, 884 (2007).

<sup>25</sup>N. Hoshino, A. M. Ako, A. K. Powell, and H. Oshio, *Inorg. Chem.* **48**, 3396 (2009).

<sup>26</sup>S.-Y. Chen, C. C. Beedle, P.-R. Gan, G.-H. Lee, S. Hill, and E.-C. Yang, *Inorg. Chem. (Washington, DC)* **51**, 4448 (2012).

<sup>27</sup>A. A. Kitos, C. G. Eftymiou, C. Papatriantafyllopoulou, V. Nastopoulos, A. J. Tasiopoulos, M. J. Manos, W. Wernsdorfer, G. Christou, and S. P. Perlepes, *Polyhedron* **30**, 2987 (2011).

<sup>28</sup>S. Koizumi, M. Nihei, T. Shiga, M. Nakano, H. Nojiri, R. Bircher, O. Waldmann, S. T. Ochsenein, H. U. Güdel, F. Fernandez-Alonso *et al.*, *Chem. Eur. J.* **13**, 8445 (2007).

<sup>29</sup>G. L. Abbati, A. Cornia, A. C. Fabretti, A. Caneschi, and D. Gatteschi, *Inorg. Chem. (Washington, DC)* **37**, 3759 (1998).

<sup>30</sup>R. W. Saalfrank, T. Nakajima, N. Mooren, A. Scheurer, H. Maid, F. Hampel, C. Trieflinger, and J. Daub, *Eur. J. Inorg. Chem.* **2005**, 1149 (2005).

- <sup>31</sup>B. Pilawa, M. T. Kelemen, S. Wanka, A. Geisselmann, and A. L. Barra, *Europhys. Lett.* **43**, 7 (1998).
- <sup>32</sup>N. C. Harden, M. A. Bolcar, W. Wernsdorfer, K. A. Abboud, W. E. Streib, and G. Christou, *Inorg. Chem. (Washington, DC)* **42**, 7067 (2003).
- <sup>33</sup>T. C. Stamatatos, D. Foguet-Albiol, K. M. Poole, W. Wernsdorfer, K. A. Abboud, T. A. O'Brien, and G. Christou, *Inorg. Chem. (Washington, DC)* **48**, 9831 (2009).
- <sup>34</sup>D. M. Pajerowski, T. C. Stamatatos, S. Mukherjee, E. S. Knowles, M. Bencomo, M. W. Meisel, and G. Christou, *Polyhedron* **29**, 2462 (2010).
- <sup>35</sup>R. Bircher, G. Chaboussant, C. Dobe, H. U. Güdel, S. T. Ochsenbein, A. Sieber, and O. Waldmann, *Adv. Funct. Mater.* **16**, 209 (2006).
- <sup>36</sup>R. Caciuffo, T. Guidi, G. Amoretti, S. Carretta, N. Magnani, P. Santini, and C. Mondelli, *Physica B* **385-386**, 301 (2006).
- <sup>37</sup>G. Shirane, R. Nathans, O. Steinsvoll, H. A. Alperin, and S. J. Pickart, *Phys. Rev. Lett.* **15**, 146 (1965).
- <sup>38</sup>J. W. Lynn, *Phys. Rev. B* **11**, 2624 (1975).
- <sup>39</sup>M. Pajda, J. Kudrnovský, I. Turek, V. Drchal, and P. Bruno, *Phys. Rev. B* **64**, 174402 (2001).
- <sup>40</sup>R. Gebauer and S. Baroni, *Phys. Rev. B* **61**, R6459 (2000).
- <sup>41</sup>D. M. Bylander, Q. Niu, and L. Kleinman, *Phys. Rev. B* **61**, R11875 (2000).
- <sup>42</sup>K. Karlsson and F. Aryasetiawan, *Phys. Rev. B* **62**, 3006 (2000).
- <sup>43</sup>R. A. Ewings, P. G. Freeman, M. Enderle, J. Kulda, D. Prabhakaran, and A. T. Boothroyd, *Phys. Rev. B* **82**, 144401 (2010).
- <sup>44</sup>J. L. Zarestky, O. Moze, J. W. Lynn, Y. Chen, T. A. Lograsso, and D. L. Schlager, *Phys. Rev. B* **75**, 052406 (2007).
- <sup>45</sup>I. Turek, J. Kudrnovský, V. Drchal, and P. Bruno, *Philos. Mag.* **86**, 1713 (2006).
- <sup>46</sup>M. Yethiraj, R. A. Robinson, D. S. Sivia, J. W. Lynn, and H. A. Mook, *Phys. Rev. B* **43**, 2565 (1991).
- <sup>47</sup>R. F. Sabiryanov and S. S. Jaswal, *Phys. Rev. Lett.* **83**, 2062 (1999).
- <sup>48</sup>O. Cépas and T. Ziman, *Prog. Theor. Phys. Suppl.* **159**, 280 (2005).
- <sup>49</sup>D. M. Low, G. Rajaraman, M. Helliwel, G. Timco, J. van Slageren, R. Sessoli, S. T. Ochsenbein, R. Bircher, C. Dobe, O. Waldmann *et al.*, *Chem.–Eur. J.* **12**, 1385 (2006).
- <sup>50</sup>O. Waldmann and H. U. Güdel, *Phys. Rev. B* **72**, 094422 (2005).
- <sup>51</sup>O. Waldmann, *Phys. Rev. B* **68**, 174406 (2003).
- <sup>52</sup>D. Gatteschi and L. Pardi, *Gazz. Chim. Ital.* **123**, 231 (1993).
- <sup>53</sup>O. Waldmann, *Phys. Rev. B* **61**, 6138 (2000).
- <sup>54</sup>J. Schnack and M. Luban, *Phys. Rev. B* **63**, 014418 (2000).
- <sup>55</sup>O. Waldmann, *Phys. Rev. B* **65**, 024424 (2001).
- <sup>56</sup>J. Schnack, M. Luban, and R. Modler, *Europhys. Lett.* **56**, 863 (2001).
- <sup>57</sup>O. Waldmann, *Coord. Chem. Rev.* **249**, 2550 (2005).
- <sup>58</sup>O. Waldmann, T. Guidi, S. Carretta, C. Mondelli, and A. L. Dearden, *Phys. Rev. Lett.* **91**, 237202 (2003).
- <sup>59</sup>S. Blundell, *Magnetism in Condensed Matter* (Oxford University Press, Oxford, UK, 2001).
- <sup>60</sup>F. A. Cotton, *Chemical Applications of Group Theory* (Wiley, New York, 1990).
- <sup>61</sup>M. Tinkham, *Group Theory and Quantum Mechanics* (Dover, New York, 2003).